JOURNAL OF THEORETICAL AND APPLIED MECHANICS
61, 2, pp. 207-218, Warsaw 2023
https://doi.org/10.15632/jtam-pl/159670

STUDY OF TRIAXIAL COMPRESSION MECHANICAL PROPERTIES AND PORE-FRACTURE CHARACTERISTICS OF COAL ROCKS IN THE YILI BASIN, XINJIANG

Cheng Shen, Ling Yue
Changzhou Vocational Institute of Engineering, Changzhou, China
Yang Liu
School of Civil and Transportation Engineering, Hebei University of Technology, Tianjin, China
e-mail: 201911601006@stu.hebut.edu.cn

Compressive mechanical properties and pore-fissure characteristics of coal rock specimens from three stably developed coal seams M_1, M_8 and M_{12} in the Xinjiang Yili Basin were investigated in detail by a series of tests. The results show that the compressive mechanical properties of coal rocks in the Yili Basin are significantly affected by the confining pressure. The peak axial stress increases and the peak modulus of elasticity decreases as the confining pressure increases. The peak axial strain increases and then remains constant, while the peak circumferential strain and peak volumetric strain increase and then decrease. The confining pressure has almost no effect on Poisson's ratio of the coal rock specimens. In addition, electron microscopy tests show that the microscopic fraction of the coal rock specimens is predominantly vitrinite, accounting for 83.1%-89.2%, while the percentage of the inertinite group is relatively small, at 10.3%-16.1%. The throat radius of the coal rock is mainly concentrated around 1-2 μm, while the pore radius of the coal rock is between 150-200 μm. The coal rock has an overall fine throat and low permeability, and the coal rock in the Yili Basin of Xinjiang is a typical low-permeability coal rock.

Keywords: triaxial compression, mechanical properties, mercury injection, pore-fissure characteristics

1. Introduction

Coal is currently one of the world's major energy sources, and its position will remain unchanged for a long time in the future. With gradual depletion of coal resources and gradual reduction of coal reserves at shallow depths, the mining of coal is subsequently moving deeper underground. Compressive mechanical properties of coal rocks are closely related to safe production of coal mines, and the study of the compressive mechanical properties of deeper coal rocks remains a priority (Wang *et al.*, 2013; Blondeel and van de Graaf, 2018; Haque *et al.*, 2018; Xu *et al.*, 2019; Shan *et al.*, 2021; Liu *et al.*, 2022).

The studies on the mechanical behavior of coal rocks have been extensively reported (Yin *et al.*, 2016; Chen *et al.*, 2019; Zhong *et al.*, 2022). Yin *et al.* (2016) studied physical and mechanical properties of coal rock after treatment at different temperatures under impact loading. Dynamic compression experiments were conducted by using a split Hopkinson pressure bar (SHPB). They found that the stress-strain curves under impact loading lacked the stage of micro-fissure closure and the slope of the elastic deformation stage was higher than that under static loading. Chen *et al.* (2019) investigated deformation and failure behavior of a coal-rock combined body under uniaxial compression by experiments and numerical simulations. Their experimental results showed that the mechanical properties and deformation failure characteristics of the coal-rock combined body were governed mainly by the coal. Zhong *et al.* (2022) investigated the role of

pore fluid in low-permeability coal away from the excavation boundary but still influenced by the periodic excavation disturbance, a series of undrained cyclic triaxial compressive tests were conducted on saturated coal. Their results showed that pore water had little effect on the axial strain evolution of coal, but has a significant effect on the radial and volumetric strain evolution.

The shape, size and surface characters of pore-fractures in coal are a basis for understanding of the occurrence and migration of coalbed methane (CBM), which requires quantitative characterization (Chen *et al.*, 2017; Zhu *et al.*, 2021; Xue *et al.*, 2022). Njiekak *et al.* (2018) studied porosity, shape and size of carbonates by a micro-computed tomography (CT) and scanning electron microscopy (SEM). Their results showed that as micro-CT porosity depended on the scan resolution and image segmentation processes, to rely solely today on micro-CT scanning for pore volume evaluation of heterogeneous carbonate samples should be considered with extreme caution. Wang *et al.* (2020) analyzed size distribution and volume contribution of pore-fractures in coal at three cohesive-scales (nanometer-scale, micrometer-scale and macro-scale) by using X-ray CT image. They found that the pore volume contribution measured using X-ray CT image analysis increased, then decreased with increasing pore diameter, and the specific surface area decreased rapidly with increasing pore diameter. Qajar and Arns (2022) studied the evolution of pore structure and permeability of a microporous carbonate rock during chemical dissolution using information provided from X-ray micro-computed tomography (μ-CT) and mercury intrusion porosimetry (MIP) techniques. They found that the permeability changes were controlled by macroporosity and critical pore diameter.

This study takes the Yili Basin, Xinjiang, as the study area, and investigates in detail the compressive mechanical properties and pore-fracture characteristics of coal specimens from three stably developed coal seams in the Yili Basin by triaxial compression tests, mercury compression tests and scanning electron microscopy tests. This will provide reference and guidance for the evaluation of recoverability and exploration and development of deep-seated coal rocks.

2. Experimental study

2.1. Sample preparation

The coal formations in the Yili Basin can be broadly divided into six systems from the bottom up, which are Triassic, Jurassic, Cretaceous, Palaeocene, Neoproterozoic and Quaternary. There are a total of 12 coal seams in the area, recorded as M_1-M_{12} from the bottom to top, of which the stable development is in seam 1 (M_1), seam 8 (M_8) and seam 12 (M_{12}). The test coal specimens were taken from each of these stable coal seams. Fresh and intact coal rock blocks were wrapped tightly in a plastic film and transported back to the laboratory, where they were then processed into standard cylindrical coal specimens of 2.5 cm diameter and 5 cm length, and numbered according to the location of the seam. The accuracy of the specimen is in accordance with the requirements of the International Society for Rock Mechanics (ISRM) (Fairhurst and Hudson, 1999), i.e. the permissible deviation of height, diameter or side length of the sample is ± 0.3 mm, the permissible deviation of unevenness of the two end faces of the sample is ± 0.05 mm, and the end faces should be perpendicular to the axis of the sample with a permissible deviation of $\pm 0.25^\circ$.

2.2. Test methods

The M_8 coal seam is between the M_1 and M_{12} coal seams, the coal rock specimens for the triaxial compression tests were taken from the M_8 seam and the tests were repeated three times under the same confining pressure. Meanwhile, both the permeability test and the component test were repeated at least three times.

2.2.1. Triaxial compression testing

The triaxial compression tests and permeability tests are carried out using the TFD-2000L triaxial rheological testing machine, which has a maximum axial load of 2000 kN and a maximum confining pressure of 200 MPa (Fig. 1a). The specific test steps are as follows: 1) The coal rock specimen was fixed to the base of the loading system and wrapped with a heat-shrinkable tube. Then heated it with a heat gun to make it tight to the coal wall, and fixed the top and bottom ends of the coal sample with sealing rings to ensure its good sealing. Then, the confining pressure chamber was closed and silicone oil was added. 2) The confining pressure control system was started to increase the confining pressure at a rate of 0.5 MPa/min. According to the sampling depth of the coal rock specimens, the confining pressures were set at to 5, 10, 15 and 20 MPa, respectively. 3) When the confining pressure reached the specified size, the coal rock sample was at hydrostatic pressure. At this point, the axial stress was applied by displacement loading with 0.01 mm/s until the specimen failure (Determination method of physical and mechanical properties of coal and rock: GB/T23561.9-2009).

2.2.2. Permeability testing

The permeability test of the coal rock specimens was also performed using the TFD-2000 triaxial rheological testing machine, which has inlet and outlet pipes at the upper and lower ends (Fig. 1b). 1) The first step was the same as the first step of triaxial compression test. 2 The axial stress and confining pressure of the coal rock specimens were maintained at 5 MPa. The vacuum pump was turned on and the coal rock specimen was vacuumed for 6 hours and the temperature was maintained at 30°C by heating the silicone oil. 3) The gas inlet valve was opened and CH4 was introduced, and the gas pressure at the inlet end was adjusted to 1.2 MPa. Gas adsorption was carried out on the coal specimen until the adsorption equilibrium was reached, and the parameters to be measured were recorded. 4) Changed the inlet pressure (1.6, 1.2, 0.8 and 0.4 MPa) and repeated steps (2), (3) and (4). 5) Based on Darcy's law, the permeability K of the coal rock can be calculated (Lin and Zhou, 1987)

$$K = \frac{2qp\mu L}{(p^2 - p_0^2)S} \tag{2.1}$$

where K is the permeability [mD]; q is the CH4 percolation flow rate at standard conditions [cm^3/s]; μ is the CH4 gas dynamic viscosity, and $\mu = 1.1502 \cdot 10^{-5}$ Pa s; L is the length of the specimen [cm]; S is the cross-sectional area of the coal rock specimen [cm^2]; p_0 is the atmospheric pressure [Pa]; p is the air pressure at the inlet end of CH4 [Pa].

2.2.3. Coal rock component testing

1) The coal specimens were crushed to less than 1.00 mm and the proportion of coal samples made less than 0.10 mm not and more than 10%. The pulverized coal was mixed with the shellac in a certain proportion, and the coal brick was made by the hot glue method, which was ground, polished and dried in order to be ready for determination. 2) The coal brick was placed under a polarized light microscope, and the difference in the characteristics of the coal rock components under the microscope was determined, and the percentage of the statistical points of each coal rock component to the total effective points was used as the final measurement result. (Method of microscopic determination of the reflectance of vitrinite in coal: GB/T 6948-2008; Determination of maceral group composition and minerals in coal: GB/T 8899-2013).

Furthermore, the Coretest ASPE730 constant velocity mercury piezometer used for mercury injection testing is capable of feeding mercury at up to 900 psi with a constant feed rate of 0.00005 ml/min and a high resolution pressure sensing acquisition device with a resolution of

0.001 psi. (Determination of pore size distribution and porosity of solid materials by mercury pressure and gas adsorption: GB/T21650-2008).

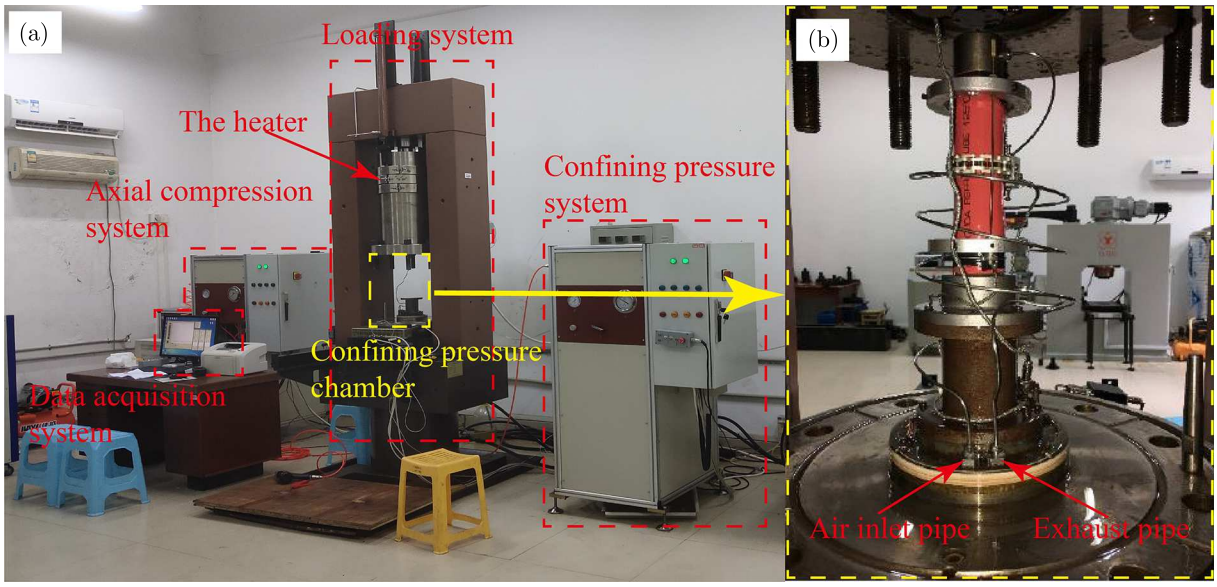

Fig. 1. Equipment for triaxial compression and penetration tests: (a) TFD-2000L triaxial rheological testing machine, (b) confining pressure chamber

3. Triaxial compression test results

3.1. Stress-strain curves

The triaxial compressive total stress-strain curves of the coal rock specimens under different confining pressures are shown in Fig. 2. It can be found that the confining pressure has a significant effect on the characteristics of the total stress-strain curves of the coal rock specimens. As shown in Fig. 2a, when the coal specimen is in uniaxial compression, the full stress-strain curve can be roughly divided into four stages, namely the initial compression-density stage, the elastic stage, the failure stage and the residual stress stage. When the coal rock specimen is in uniaxial compression, its initial stress increases rapidly, while the axial strain increases slowly, and the stress-strain curve is initially straight and then slightly curved. When the coal sample enters the second stage, the elastic state, the stress-strain curve is a straight line segment. When the specimen reaches the peak load and damage occurs, the axial stress drops significantly, followed by the residual stress phase. As shown in Fig. 2b, the full stress-strain curve of a coal sample under confining pressure can be roughly divided into three stages, namely the initial compression-density stage, the plastic stage and the damage stage. The stress-strain curve for the coal rock under confining pressure conditions has no obvious elastic segment, and as the stress increases the curve shows a clear non-linearity with a typical plastic deformation phase. The coal sample then breaks down and the stress decreases with no residual stress stage.

3.2. Peak strain and peak stress

The peak mechanical parameters of the triaxial compression of the coal rock under different confining pressures are shown in Fig. 3, and the basic mechanical parameters are listed in Table 1. From Fig. 3a and Table 1, it can be seen that the influence of the confining pressure on the peak axial stress of the coal rock specimen is very obvious. When the confining pressure is 0 MPa, the peak axial stress is 2.85 MPa, and when the confining pressure is 5 MPa, the peak axial stress is

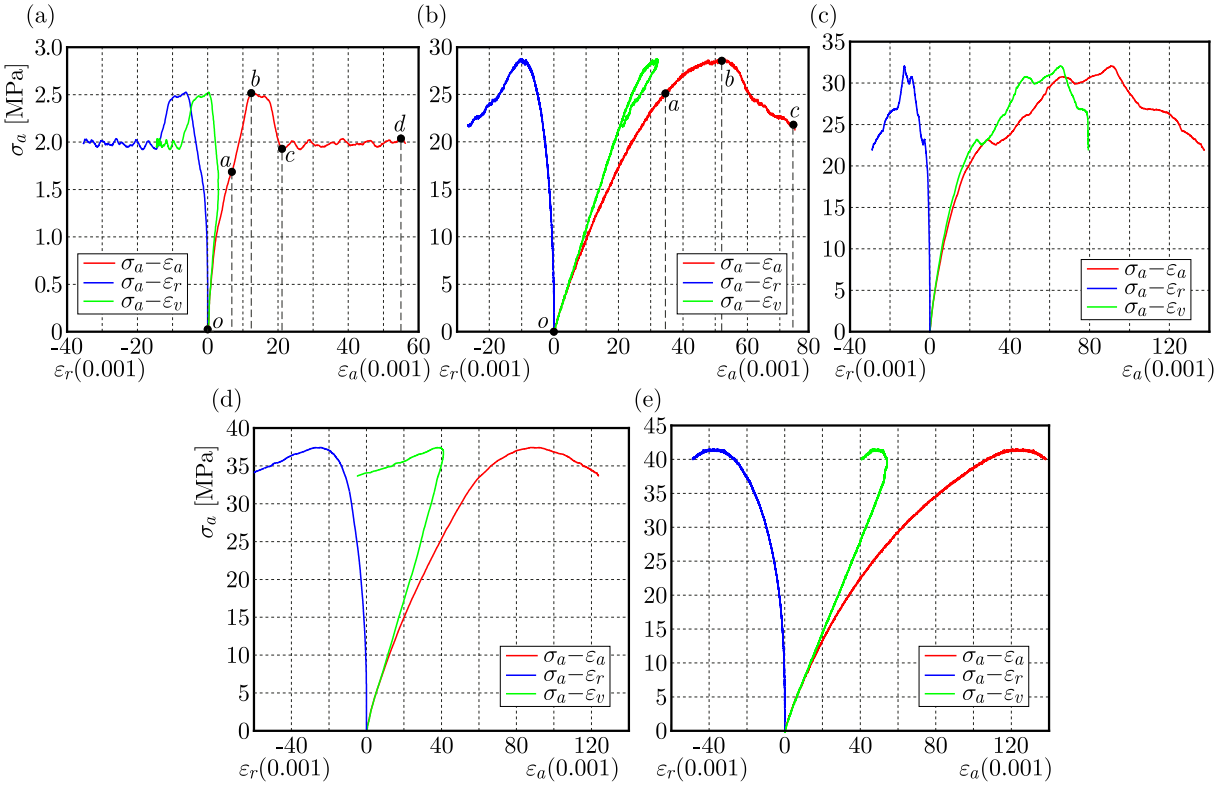

Fig. 2. Triaxial compression total stress-strain curves for coal rock specimens at different confining pressures: (a) 0 MPa, (b) 5 MPa, (c) 10 MPa, (d) 15 MPa, (e) 25 MPa

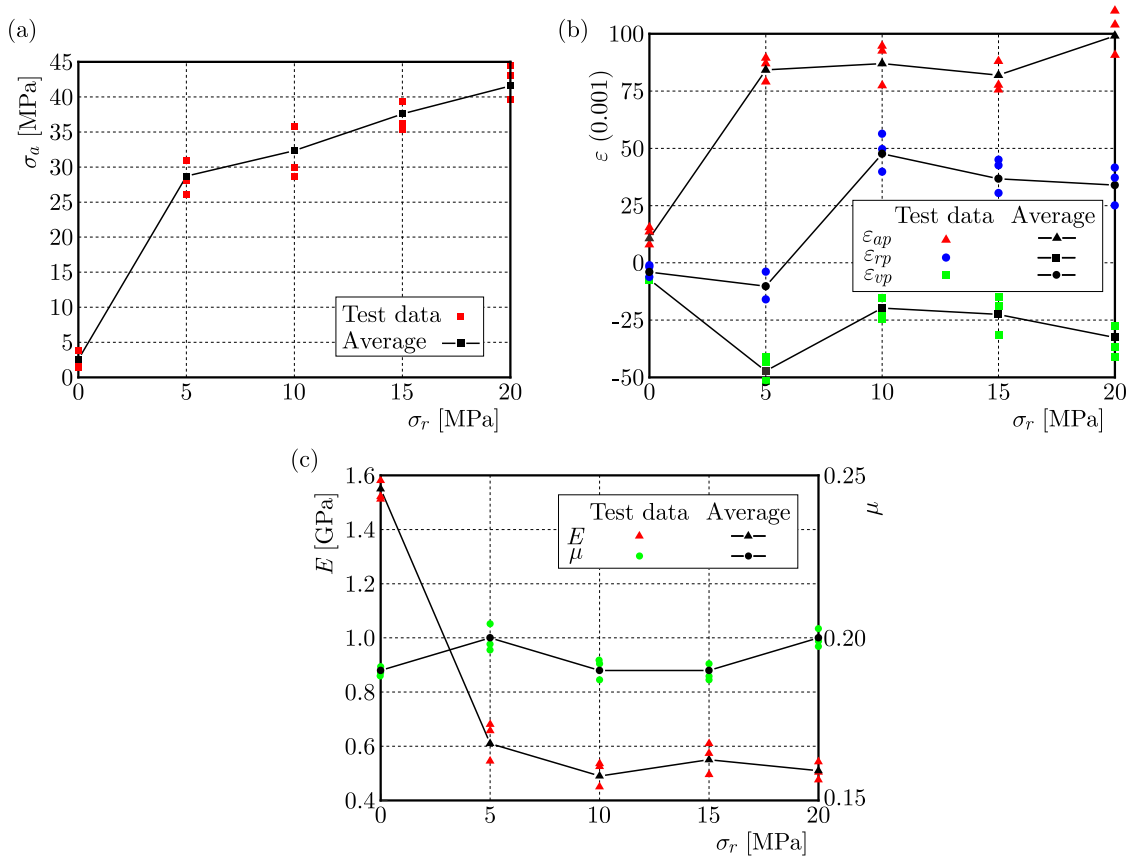

Fig. 3. Relationship between peak mechanical parameters and confining pressure: (a) axial stress, (b) strain, (c) elastic modulus and Poisson's ratio

27.81 MPa, which is an increase by 9.76 times. At the same time, it can be found that the rate of increase of the peak axial stress in the coal rock decreases significantly with the gradual increase of the confining pressure. This indicates that although the confining pressure can significantly increase the peak axial stress in the coal rock, the rate of increase is limited.

The trend of the peak strain of the coal rock with the confining pressure is shown in Fig. 3b. The peak axial strain increases rapidly with an increase of the confining pressure and then remains almost constant. The peak circumferential strain, on the other hand, increases first and then decreases with increasing confining pressure, reaching a maximum value when the confining pressure is 5 MPa. The peak volumetric strain increases from negative to positive with the increasing confining pressure, which indicates that the peak volumetric strain is determined by the peak circumferential strain at 0-5 MPa and the peak volumetric strain is determined by the peak axial strain when the confining pressure is 10-20 MPa.

The relationship among the peak modulus of elasticity and the peak Poisson's ratio and the confining pressure is shown in Fig. 3c. The peak modulus of elasticity of the coal rock decreases significantly with an increase of the confining pressure, i.e. the peak modulus of elasticity of the coal rock achieves the maximum value at 0 MPa, which is due to the presence of the confining pressure which makes the axial strain of the coal rock increase significantly during the compression process, however, the axial stress cannot increase proportionally with the axial strain. For Poisson's ratio of the coal rock, which remains between 0.18 and 0.21, the effect of the confining pressure on the modulus of elasticity of the coal rock is relatively small.

Table 1. Basic mechanical parameters of coal rock specimens under different confining pressures

σ_r [MPa]	σ_{ap} [MPa]	ε_{ap} [0.001]	ε_{rp} [0.001]	ε_{vp} [0.001]	E [GPa]	μ
0	2.85	11.76	−7.63	−4.23	1.51	0.18
5	27.81	82.21	−46.68	−12.36	0.58	0.20
10	33.25	85.69	−18.74	45.51	0.51	0.19
15	36.98	82.73	−24.37	34.24	0.54	0.21
20	42.37	98.48	−35.89	31.61	0.56	0.20

Note: σ_r is the confining pressure
σ_{ap} is the peak axial strength
ε_{ap} is the peak axial strain
ε_{rp} is the peak circumferential strain
ε_{vp} is the peak volume strain
E is the elastic modulus, μ is Poisson's ratio

3.3. Ultimate failure pattern

The triaxial compression damage pattern of the coal rock specimens is shown in Fig. 4. Oblique shear damage and vertical splitting damage are the main forms of damage to the coal rock. Moreover, the degree of coal rock fragmentation significantly increases with an increase of the confining pressure. This indicates that although high confining pressure can effectively increase the load capacity and deformation capacity of the coal rock, once the coal rock is damaged, the energy released and the degree of fragmentation will also increase significantly. As a result, the coal rock needs to be mined more safely and cautiously under high confining pressure.

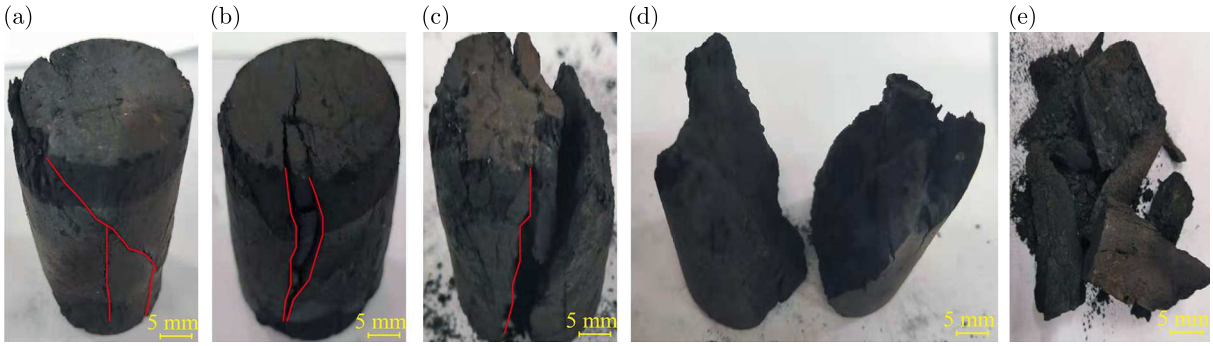

Fig. 4. Triaxial compression failure patterns of coal rock under different confining pressure

4. Mercury pressure testing and pore-fracture characterisation

4.1. Capillary pressure

The capillary pressure curves of the coal rocks obtained from the mercury pressure tests are shown in Fig. 5. The capillary pressure curve of the coal specimen is generally located in the upper left part of the figure, which indicates that the physical properties of the coal rocks in the Yili Basin of Xinjiang are generally poor and the permeability is small. The capillary pressure curve increases significantly with increasing mercury saturation, with no obvious flattening trend throughout the process. The rate of capillary pressure increase is significantly faster when the mercury saturation is between 0-20%. When the mercury saturation is above 20%, the rate of capillary pressure increase slows down significantly, indicating poor pore radius sorting in the coal rock specimens. This differs significantly from the capillary pressure curves obtained for other more common higher-order coal and sandstone reservoirs, which typically have more significant flat segments. Furthermore, the overall sortability of the conventional sandstone and high-order coal reservoirs is better and is usually dominated by the development of pore fractures, the main feature being the larger volume and greater number of pores within their coal rocks. In contrast, for the lower-order coals, the microfractures within the coal specimens are relatively underdeveloped and the pore-fissure radii are overall poorly sorted, forming a curve pattern that projects to the upper left.

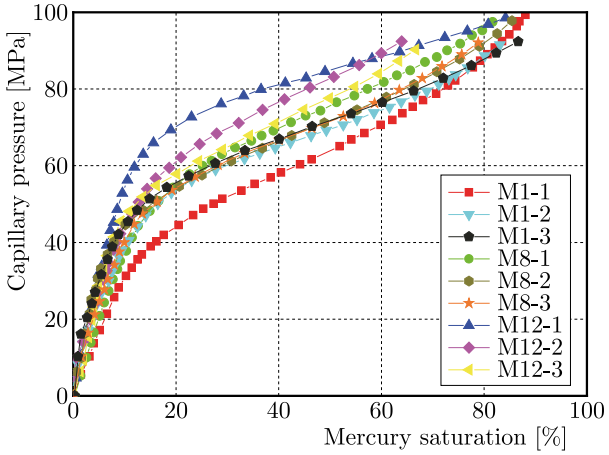

Fig. 5. High pressure mercury capillary pressure curve for 9 coal specimens

The input and output mercury curves of the coal rock specimens are shown in Fig. 6. The input and output mercury curves from the three stably developed coal seams in the Yili Basin, Xinjiang, are generally similar. Among them, the cumulative mercury intrusion of the coal rock

specimens is in descending order for the M_8, M_1 and M_{12} seams. This indicates that the pore space in the M_8 seam is slightly larger than that in the M_1 and M_{12} seams. In addition, all three groups of coal rock specimens have a small portion of the mercury withdrawal curve overlapping with the mercury ingress curve at the beginning of the mercury withdrawal, and the hysteresis loop formed by the mercury ingress and egress curves is small, indicating that the coal rock specimens have fewer open pores and are less connected.

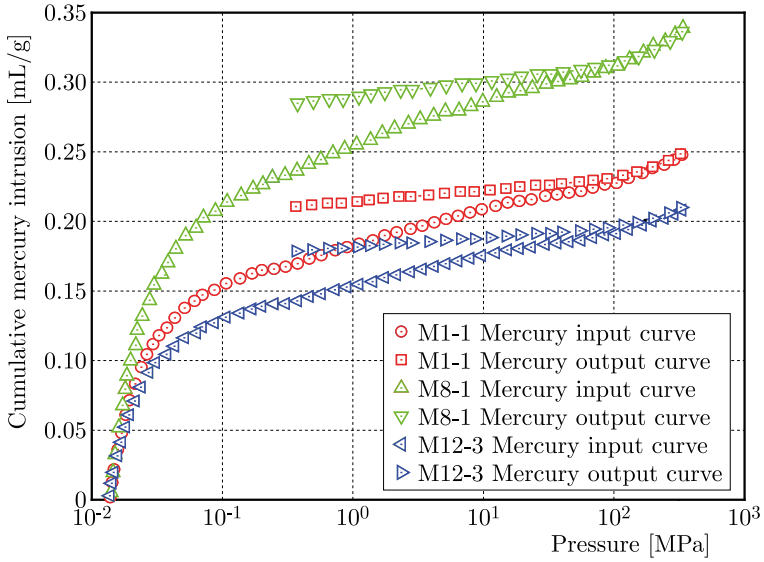

Fig. 6. Mercury-dehydration curves of three coal rock specimens

4.2. Throat and pore distribution characteristics

The pore volumes of the three groups of coal specimens are shown in Fig. 7, which shows a typical single-peak structure with peaks mainly in the range of 104-105 nm. The pore volumes of the three groups of coal specimens are significantly different, with the pore volumes from the M_8 seam being significantly larger than those from the M_1 and M_{12} seams. This trend is consistent with the variation pattern of the pressure-relief curve in Fig. 6. The analysis by the Hodot quadratic method (Yang *et al.*, 2020) shows that the pore volume of coal rock specimens from the Yili Basin, Xinjiang, is 38.6% microporous, 36.8% small porous, 11.5% medium porous and only 13.1% large porous, and the pores of coal rocks are dominated by microporous and small pores.

Based on the mercury-pressure tests, the distribution of throat radii and pore radii of coal rocks in the Yili Basin, Xinjiang, is shown in Figs. 8 and 9. From Fig. 8 it can be seen that the throat radii of the three stably developed coal seams, M_1, M_8 and M_{12}, are mainly concentrated around 1-2 μm, which indicates that the overall throat radii of coal rocks are on the fine side, thus leading to the overall low permeability of coal rocks. On the other hand, the pore radius is between 150-200 μm, which indicates that the small micropores and medium are more developed in the coal rocks, while the fine throat channels are more distributed and the pores are mostly fine necked bottle pores with poor pore connectivity, which is not conducive to the storage and desorption of coalbed methane (CBM). Figure 10 shows the pore-throat ratio of coal rock specimens. The pore-throat ratio reflects the configuration relationship between pore and throat. The distribution of the pore-throat ratio is opposite to that of throat channel, the higher the permeability of coal rock specimens, the more concentrated the distribution of the pore-throat ratio.

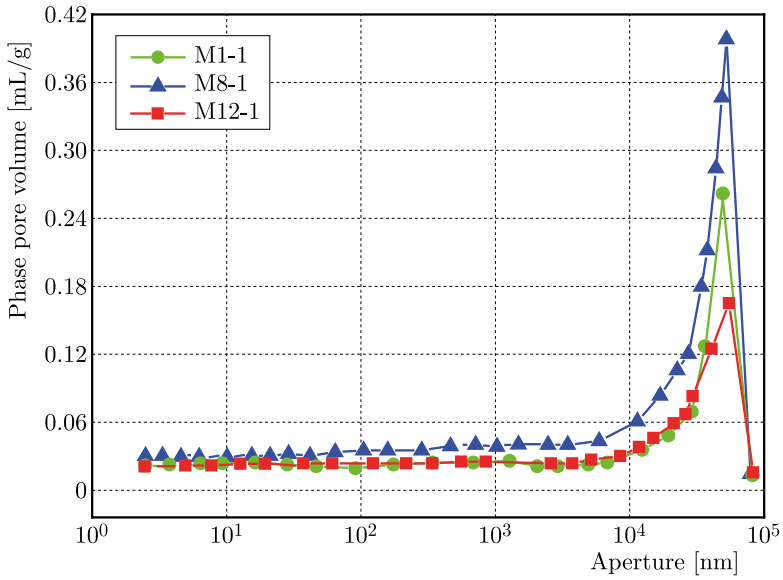

Fig. 7. Pore volume relationship for three sets of coal rock specimens

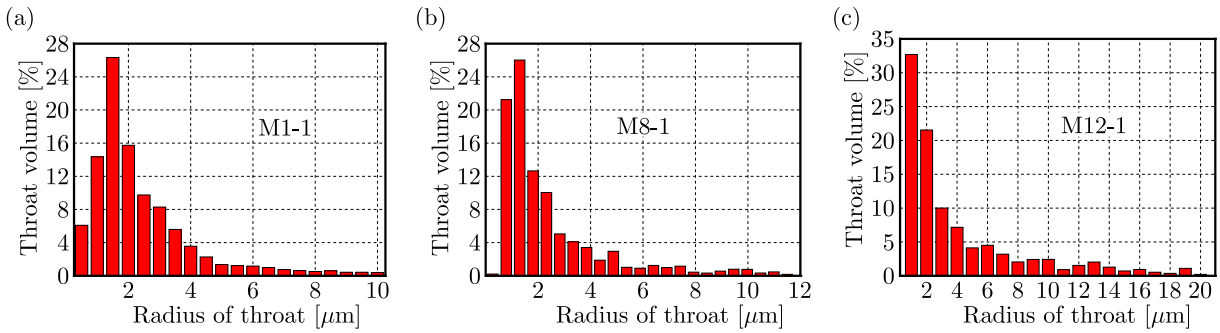

Fig. 8. Characteristics of the distribution of throat radii in coal rock specimens

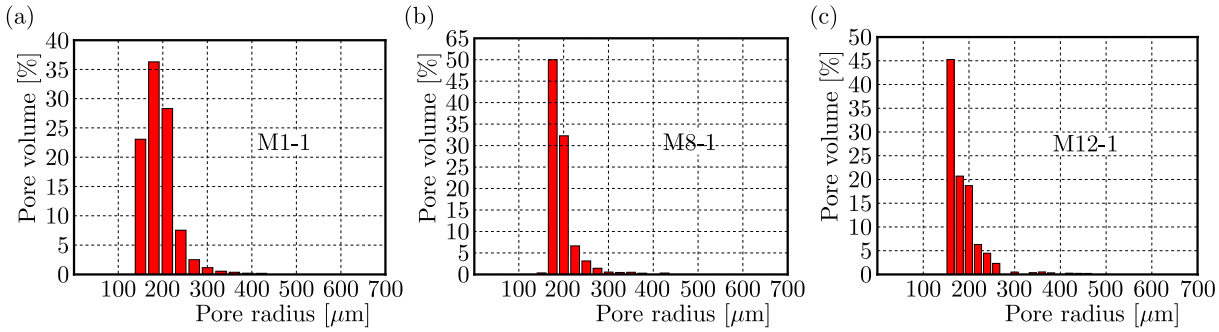

Fig. 9. Pore radius distribution characteristics of coal rock specimens

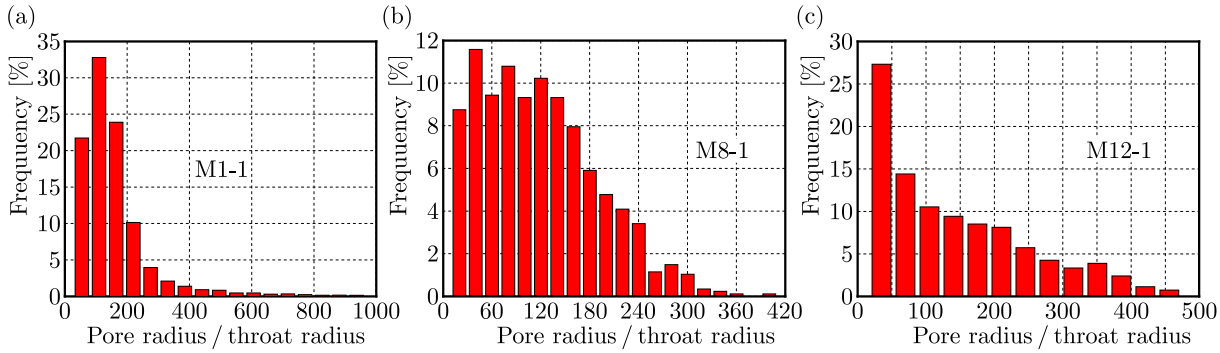

Fig. 10. The pore-throat ratio of coal rock specimens

4.3. Maximum reflectance characteristics of the coal rock microfraction and specular group

The basic physical parameters of the coal specimens are shown in Table 2. Among them, the permeability of the six coal rock specimens in the M_1 and M_{12} seams ranged from 0.11-0.19 mD, which is a medium permeability reservoir. The permeability of the coal rock specimens in the M_8 seam ranged from 0.06-0.09 mD, which is typical for low permeability reservoirs. In addition, the porosity of the nine coal rock specimens ranged from 4.1% to 5.5%, with an average porosity of 4.98%, which is typical for low porosity reservoirs. The porosity range of the coal sample specimens indicates that the overall physical properties of the coal rocks in the Yili Basin of Xinjiang are poor.

Table 2. Basic physical parameters of coal specimens

Specimen number	Porosity [%]	Penetration rate [mD]	Density [g/cm^3]	Maximum specular body reflectance [%]	Vitrinite [%]	Inertinite [%]	Chitinous [%]
M_1-1	4.9	0.11	0.92	3.52	83.1	16.1	0.8
M_1-2	5.2	0.13	0.84	2.67	86.7	13.0	0.3
M_1-3	4.1	0.14	0.88	3.62	86.3	13.2	0.5
M_8-1	5.3	0.07	0.96	3.13	84.5	15.1	0.4
M_8-2	4.5	0.09	0.91	3.47	86.5	13.1	0.4
M_8-3	5.5	0.06	0.89	3.59	89.2	10.3	0.5
M_{12}-1	4.8	0.18	0.87	3.64	88.2	11.4	0.4
M_{12}-2	5.1	0.17	0.93	3.17	85.6	14.3	0.1
M_{12}-3	5.4	0.19	0.97	3.01	86.4	13.1	0.6

Meanwhile, the test results show that the microscopic fraction of the coal rocks in the Yili Basin, Xinjiang, is dominated by vitrinite, with a percentage of 83.1%-89.2 and an average of 86.27%, while the percentage of the inert group is relatively small, with its percentage ranging from 10.3%-16.1%. It can also be seen that for the coal rock specimens tested, the chitinous group is very small, at just 0.1%-0.8%. In addition, small amounts of carbonate minerals and clay minerals were found in the coal specimens.

5. Discussion

A large amount of gas is formed during formation of coal, and effective gas extraction can reduce the gas content and pressure to a safe range, thus reducing the possibility of gas disaster accidents. As the depth of the coal seam increases, the confining pressure on the coal rock increases. There is a large number of original defects (micro-fractures and micro-porosity) inside the coal rock specimens, and these original defects are highly susceptible to compressive deformation under the action of external stress. As the confining pressure continues to increase, the original defects are further compressed and closed, and the coal matrix squeezes the micro-pore fracture space inward, which leads to the narrowing of the seepage channel and the obstruction of gas transport in the micro-pore fracture space (Gray, 1987). The coal seam permeability characteristics will directly affect the gas extraction efficiency of the mine. In this study, the permeability of coal rock specimens under fixed confining pressure conditions was investigated, however, the effect of different confining pressure on the permeability of coal rock specimens was not considered. Therefore, the influence of different confining pressure on the permeability of coal rock specimens will be emphasized in the next work.

6. Conclusion

In this paper, the triaxial mechanical properties and pore-fracture characteristics of coal rocks in the Yili Basin, Xinjiang, were investigated by triaxial compression tests, mercury compression tests and scanning electron microscopy tests. The following main conclusions were obtained.

- Confining pressure has a significant effect on the compressive mechanical properties of coal rocks in the Yili Basin, Xinjiang. As the confining pressure increases, the axial peak stress of coal rocks increases, while the peak elastic modulus decreases significantly. The axial peak strain increases and then remains constant, while the circumferential peak and volumetric peak strains increase and then decrease. The confining pressure has almost no effect on Poisson's ratio of the coal rock specimens.
- Oblique shear damage and vertical splitting damage are the main forms of damage to the coal rock. Furthermore, the degree of coal rock fragmentation increases significantly with the increase of the confining pressure.
- The microscopic fraction of coal rocks in the Yili Basin of Xinjiang is dominated by the mirror mass, with a proportion of 83.1%-89.2, while the proportion of the inert group is relatively small, with its proportion ranging from 10.3%-16.1%. In addition, the coal rocks are generally typical low-permeability coal rocks with permeabilities ranging from 0.06-0.19 mD and poor pore connectivity.

It is worth noting that the micro fissure-pores of coal rock specimens are closely related to their petrographic composition. Therefore, enough attention should be paid in the related future studies.

Acknowledgments

This work was supported by the National Natural Science Foundation of China (No. 51638002), and the Natural Science Foundation of Jiangsu Province Universities Project (No. 19KJD410001).

References

1. Blondeel M., van de Graaf T., 2018, Toward a global coal mining moratorium? A comparative analysis of coal mining policies in the USA, China, India and Australia, *Climatic Change*, **150**, 89-101
2. Chen S., Yang T., Ranjith P.G., Wei C., 2017, Mechanism of the two-phase flow model for water and gas based on adsorption and desorption in fractured coal and rock, *Rock Mechanics and Rock Engineering*, **50**, 571-586
3. Chen Y.L., Zuo J.P., Liu D.J., Wang Z., 2019, Deformation failure characteristics of coal-rock combined body under uniaxial compression: experimental and numerical investigations, *Bulletin of Engineering Geology and the Environment*, **78**, 3449-3464
4. Fairhurst C.E., Hudson J.A., 1999, Draft ISRM suggested method for the complete stress--strain curve for the intact rock in uniaxial compression, *International Journal of Rock Mechanics and Mining Sciences*, **36**, 3, 279-289
5. Gray I., 1987, Reservoir engineering in coal seams, Part 1 – The physical process of gas storage and movement in coal seams, *SPE Reservoir Engineers*, **2**, 1, 28-34
6. Haque E., Reza S., Ahmed R., 2018, Assessing the vulnerability of groundwater due to open pit coal mining using DRASTIC model: a case study of Phulbari Coal Mine, Bangladesh, *Geosciences Journal*, **22**, 359-371
7. Lin B.Q., Zhou S.N., 1987, Experimental study on gas permeability of coal sample, *Journal of China University of Mining and Technology*, **16**, 2, 21-28

8. Liu Y., Lu C.P., Xiao Z.Y., Guo Y., 2022, Mechanisms underlying the slip and failure of coal-rock parting-coal sructures under unloading conditions, *Rock Mechanics and Rock Engineering*, **55**, 4913-4928

9. National Standardization Administration Committee, 2008, Determination of pore size distribution and porosity of solid materials by mercury pressure and gas adsorption: GB/T21650-2008. Beijing: Standards Press of China

10. National Standardization Management Committee, 2008, Method for microscopic determination of specular reflectance of coal: GB/T6948-2008. Beijing: Standards Press of China

11. National Standardization Administration Committee, 2009, Determination method of physical and mechanical properties of coal and rock: GB/T23561.9-2009. Beijing: Standards Press of China

12. National Standardization Administration Committee, 2013, Determination of maceral group composition and minerals in coal: GB/T 8899-2013. Beijing: Standards Press of China.

13. Njiekak G., Schmitt D.R., Kofman R.S., 2018, Pore systems in carbonate formations, Weyburn field, Saskatchewan, Canada: Micro-tomography, helium porosimetry and mercury intrusion porosimetry characterization, *Journal of Petroleum Science and Engineering*, **171**, 1496-1513

14. Qajar J., Arns C.H., 2022, A comparative study of micro-CT and mercury intrusion techniques for predicting permeability and surface area evolution during chemical dissolution, *Advances in Water Resources*, **168**, 104301

15. Shan R.L., Li Z.L., Wang C.H., Wei Y., Tong X., Liu S., Shan Z., 2021, Study on the distribution characteristics of stress deviator in the surrounding rock when mining closely spaced coal seams, *Environmental Earth Sciences*, **80**, 602

16. Wang L., Cheng Y.P., Xu C., An F.H., Jin K., Zhang X.L., 2013, The controlling effect of thick-hard igneous rock on pressure relief gas drainage and dynamic disasters in outburst coal seams, *Natural Hazards*, **66**, 1221-1241

17. Wang X.L., Pan J.N., Wang K., Ge T., Wei J., Wu W., 2020, Characterizing the shape, size, and distribution heterogeneity of pore-fractures in high rank coal based on X-ray CT image analysis and mercury intrusion porosimetry, *Fuel*, **282**, 15, 118754

18. Xu C., Fu Q., Cui X.Y., Wang K., Zhao Y., Cai Y., 2019, Apparent-depth effects of the dynamic failure of thick hard rock strata on the underlying coal mass during underground mining, *Rock Mechanics and Rock Engineering*, **52**, 1565-1576

19. Xue Y., Liu J., Ranjith P.G., Gao F., Xie H., Wang J., 2022, Changes in microstructure and mechanical properties of low-permeability coal induced by pulsating nitrogen fatigue fracturing tests, *Rock Mechanics and Rock Engineering*, **55**, 74697488

20. Yang J., Zhang Z., Zhao L.F., 2020, Study on pore-fracture characteristics of coal rocks in the Buri Basin, *Coal Mine Safety*, **51**, 12, 214-218

21. Yin T.B., Wang P., Li X.B., Shu R.H., Ye Z.Y., 2016, Effects of thermal treatment on physical and mechanical characteristics of coal rock, *Journal of Central South University*, **23**, 2336-2345

22. Zhong C.L., Zhang Z.Y., Ranjith P.G., Zhang C., Xue K., 2022, The role of pore pressure on the mechanical behavior of coal under undrained cyclic triaxial loading, *Rock Mechanics and Rock Engineering*, **55**, 1375-1392

23. Zhu H.X., Han L.J., Meng Q.B., Liu J., Meng L., Dong W., 2021, The split-permeation grouting mechanism of loose and broken coal rock masses considering the temporal and spatial characteristics of slurry viscosity, *KSCE Journal of Civil Engineering*, **25**, 1887-1900

Manuscript received September 11, 2022; accepted for print December 7, 2022